

# TIME TRANSFER USING TIME REVERSAL ( $T^3R$ )

Eung-Gi Paek<sup>1</sup>, Joon Y. Choe<sup>2</sup>, and Ronald L. Beard<sup>1</sup>

<sup>1</sup> Naval Research Laboratory, Washington, D.C.

<sup>2</sup> ONR Global

## Abstract

We describe a new time-transfer method using time reversal processing operated at a pre-defined period. The method has a potential to transfer time with high precision, without being affected by the undesired delays or distortion caused by propagation, multipath and instrumentation. Experimental results of the proposed time transfer concept, its applications to multiple user support, and long-distance time transfer using the ionosphere will be demonstrated.

## INTRODUCTION

Time transfer permits multiple users at long distances to share a precise reference time. It has many modern applications such as very long baseline interferometry (VLBI), multistatic radars, power plants, cellular phone, etc. Various methods have been developed, including one-way, two-way, and common-view, mostly relying on GPS [1].

Time reversal or phase conjugation [2-4] has the capability to self-focus a beam both spatially and temporally. However, there has been little work reported on the use of time reversal for time transfer applications. The work by Lu *et al.* [5] operates like the conventional two way technique requiring coordination and exchange of data.

In this paper, we describe a new time transfer method based on time reversal [6,7]. By operating time reversal repeatedly at a pre-defined period, one can transfer time with high precision without being affected by the undesired delays or distortion caused by propagation, multipath and instrumentation. The most striking feature of our synchronization method is that it can effectively decouple propagation delay and time offset, and result in only the desired time offset. We present several experimental results demonstrating the proposed time transfer concept, along with other features such as simultaneous multiple user support in a multipath environment including the ionosphere.

## I. OPERATIONAL PRINCIPLE OF $T^3R$

Figure 1(a) shows the basic operation of the proposed  $T^3R$  scheme between a user and a reference node. The reference node is a service provider and has a time reversal mirror (TRM). First, a user sends out a short pulse to the reference node. The received signal at the reference node is delayed by propagation delay,  $p$ , and is distorted to  $h(t)$  by the intermediate medium, where  $h(t)$  is an impulse response of the propagation channel. The received signal is then time-reversed to  $h(-t)$  and is retransmitted back to the user. Assuming that the medium is reciprocal, the signal received by the user is given by the autocorrelation of  $h(t)$ . Since it is an autocorrelation, the waveform is symmetric with respect to a unique central peak.

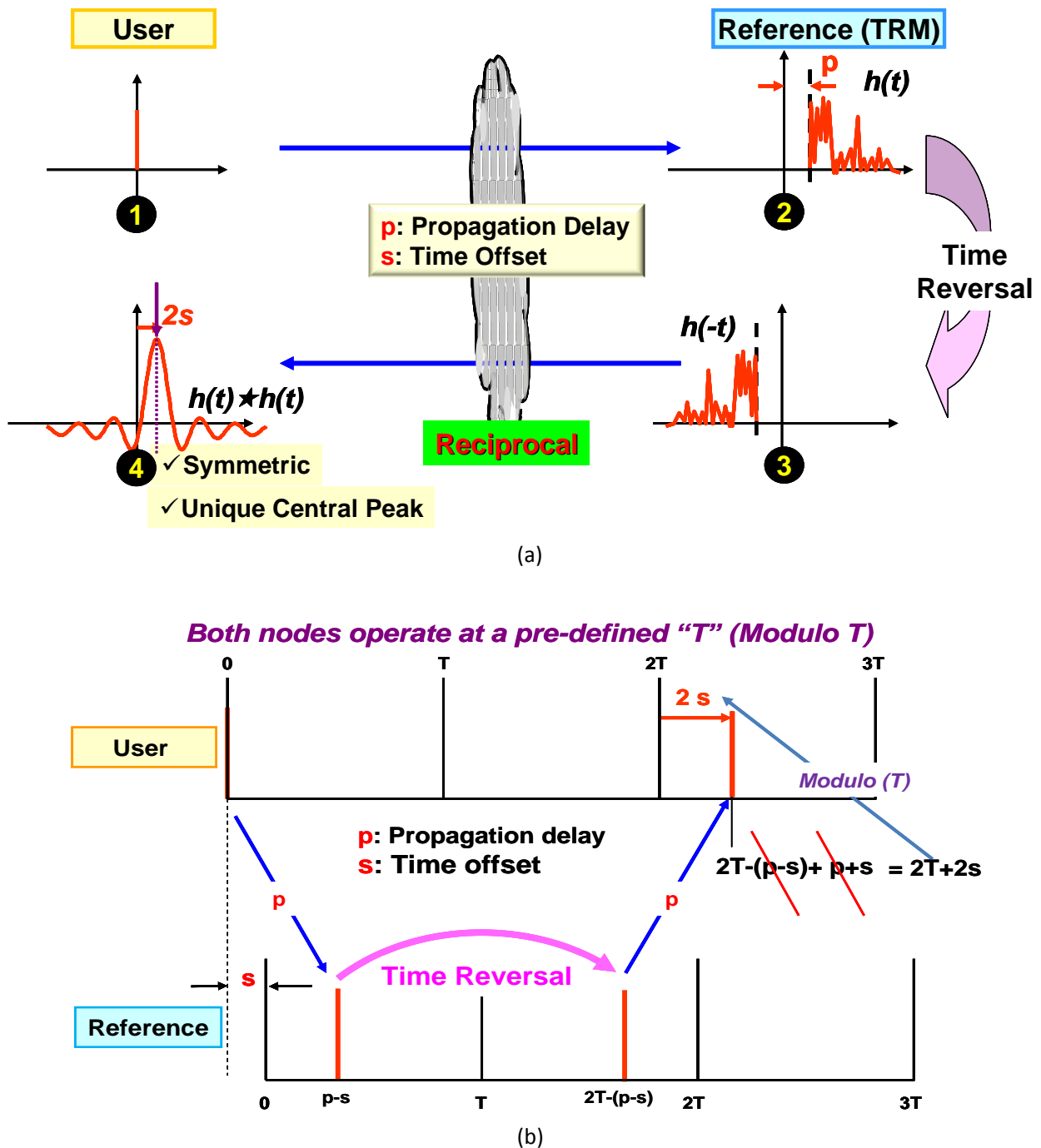


Figure 1. Time Transfer using Time Reversal (T<sup>3</sup>R): (a) operational principle; (b) “ $p$ ”-independence.

The peak location can then be determined without ambiguity. The scheme does not require coordination or the exchange of data between the nodes. Also, the system is tolerant to multipath interference or other signal distortion. These effects make the impulse response more complicated (or broader bandwidth) and contribute to sharpening the correlation peak. So, in this case, the multipath effects help rather than hurt the system performance. Finally, the autocorrelation peak appears at  $2s$  ( $s$  is time offset of the user.), regardless of propagation delay,  $p$ , as explained below.

Figure 1(b) illustrates the timing relationship between user and reference nodes. Both nodes operate at a pre-defined period  $T$ . Here again,  $p$  represents the one-way propagation delay between the nodes and  $s$  is the time offset of the user node with respect to the reference node. The user sends out a short pulse at  $t=0$  in user time. After  $p$  seconds the reference node receives the pulse at  $p-s$  in reference time. The frame (0 to  $T$ ) is time reversed with respect to  $T$  to the next frame ( $T$  to  $2T$ ), generating a pulse at  $2T-(p-s)$ . The time reversed signal is retransmitted back to the user. The user receives the pulse at  $2T-(p-s)+p+s = 2T+2s$  in user time. Note that  $p$  has been canceled out. Also, noting that user node updates its frame every period  $T$ , the pulse appears at modulo  $(2T+2s, T) = 2s$ . Therefore, user node receives the returned signal at  $2s$  – independently of propagation delay. This concept is called “ $p$ ”-independence and constitutes the main subject of this paper.

Here we assumed that the period is constant and same for both nodes. Assuming that the Allan deviation of the clock at  $\tau=T$  is 1.0E-9, and the period  $T$  is 1 ms, the error in  $2T$  becomes  $2*1.0E-9*1$  ms=2 ps, which is normally smaller than the required resolution.

## II. EXPERIMENTAL DEMONSTRATION OF “P”-INDEPENDENCE

To prove the concept of the proposed “ $p$ ”-independence, we set up a system using commercially available off-the-shelf (COTS) components and instruments, as shown in Figure 2(a).

First, the user generates a pulse waveform signal with a PC and loads it into an arbitrary waveform generator (AWG, Tektronix Arbitrary Function Generator, Model AFG3022B). A short pulse or a frequency modulated continuous wave (FMCW) at a carrier frequency of about 10 MHz was used in these experiments. The AWG then generates a trigger signal with a period  $T$ , and at each rising edge of the trigger signal, the pulse waveform is generated.

Special care must be taken to ensure that the phase of the signal waveform is constant with respect to the trigger signal across the pulses. For that, the trigger signal is generated at CH2 with the same AWG, which is then input to TRIG IN port and the resultant TRIG OUT signal is used to trigger both the pulse waveform generation and the oscilloscope (Tektronix, Digital Phosphor Oscilloscope, Model DPO4104).

To phase lock and to keep the period  $T$  same between the two remote nodes (within the time on the order of the period), a Rubidium clock (SRS, Rubidium Frequency Standard, Model FS725) was used to phase lock the AWG at each node. Finally to generate a desired amount of time offset “ $s$ ” in this test, a delay generator (SRS, Digital Delay/Pulse generator, Model DG645) was used at the user node.

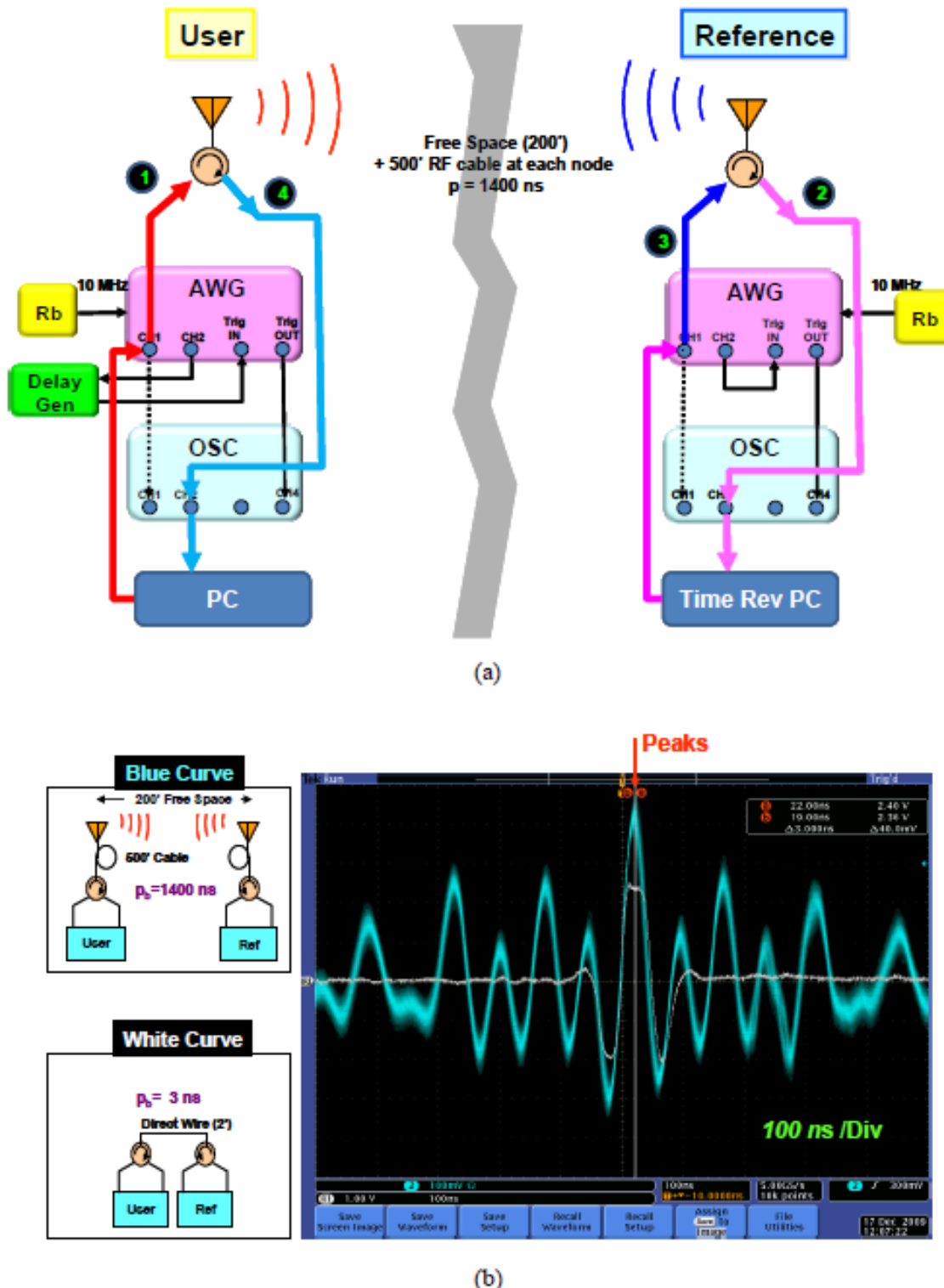


Figure 2. An experimental demonstration of “ $p$ ”-independence: (a) experimental setup; (b) results.

A series of the pulse signals was then repeatedly transmitted from the user's monopole antenna. At the reference node, which consists of the same components as the user (except for a delay generator), the received signal is digitized by an oscilloscope, read and time reversed with a PC, loaded back into an AWG, and retransmitted to the user. The user receives the returning signal at CH2 and compares it with the originally transmitted signal at CH1 to measure the time offset  $s$ . To increase the signal-to-noise ratio (SNR), the received signal is averaged with an oscilloscope, as will be explained in Section VI.

In this setup, the user and reference nodes were separated by 50ft of free space and long cables at each ends, so the propagation delay is  $p = 1400$  ns or  $1.4 \mu\text{s}$ . Also, the time offset  $s$  was set to 10 ns. Figure 2(b) shows the experimental result. The returning waveform (shown in blue curve) was symmetric with respect to a unique central peak at around 20 ns, which is twice the time offset  $s$ , as expected.

To prove “ $p$ ”-independence further, we connected the two nodes directly with a short cable, which corresponds to a propagation delay of around 3 ns. The resultant waveform (shown in the white curve) was also symmetric with respect to a central peak at  $2s$ . So, we have seen that the signals through two different paths (1400 ns and 3 ns) arrive at the same time,  $2s$ , after round-trip, demonstrating the “ $p$ ”-independence.

### III. MITIGATION OF INTEGER AMBIGUITY

To avoid the well-known integer ambiguity problem associated with carrier phase detection, we use the following frequency dithering based on “ $p$ ”-independence.

The sequence of events illustrated in Figure 3(a) is as follows. First, the user sends out a waveform (shown in blue curve) with a carrier frequency  $f_1$  and a gaussian envelope with its true central peak at  $t=0$ . After round trip from the reference node, user receives the signal with its true peak at  $2s$ . Next, the user generates a second wave (shown in red curve) with a different carrier frequency,  $f_2$ , while maintaining its central true peak is at  $t=0$ . After the round-trip, the returning signal appears with its true central peak at  $2s$ , as shown in the figure. Other false peaks will shift accordingly in the opposite directions with respect to the central peak.

Figure 3(b) shows an experimental result using this technique obtained from the system shown in Figure 2(a). Carrier frequencies used in this test were  $f_1=8.5$  MHz and  $f_2=11.5$  MHz. One can see that the experimental result agrees with the theoretical prediction discussed above.

It can be seen that “ $p$ ”-independence allows the location of the true peak to be fixed at  $2s$ , regardless of the frequencies used (to the extent of the dispersion limit), whereas other side peaks shift outwards from the true peak and are out of phase with each other. So, simply by averaging after choosing proper frequencies, one can significantly reduce false peaks without degrading the true peak.

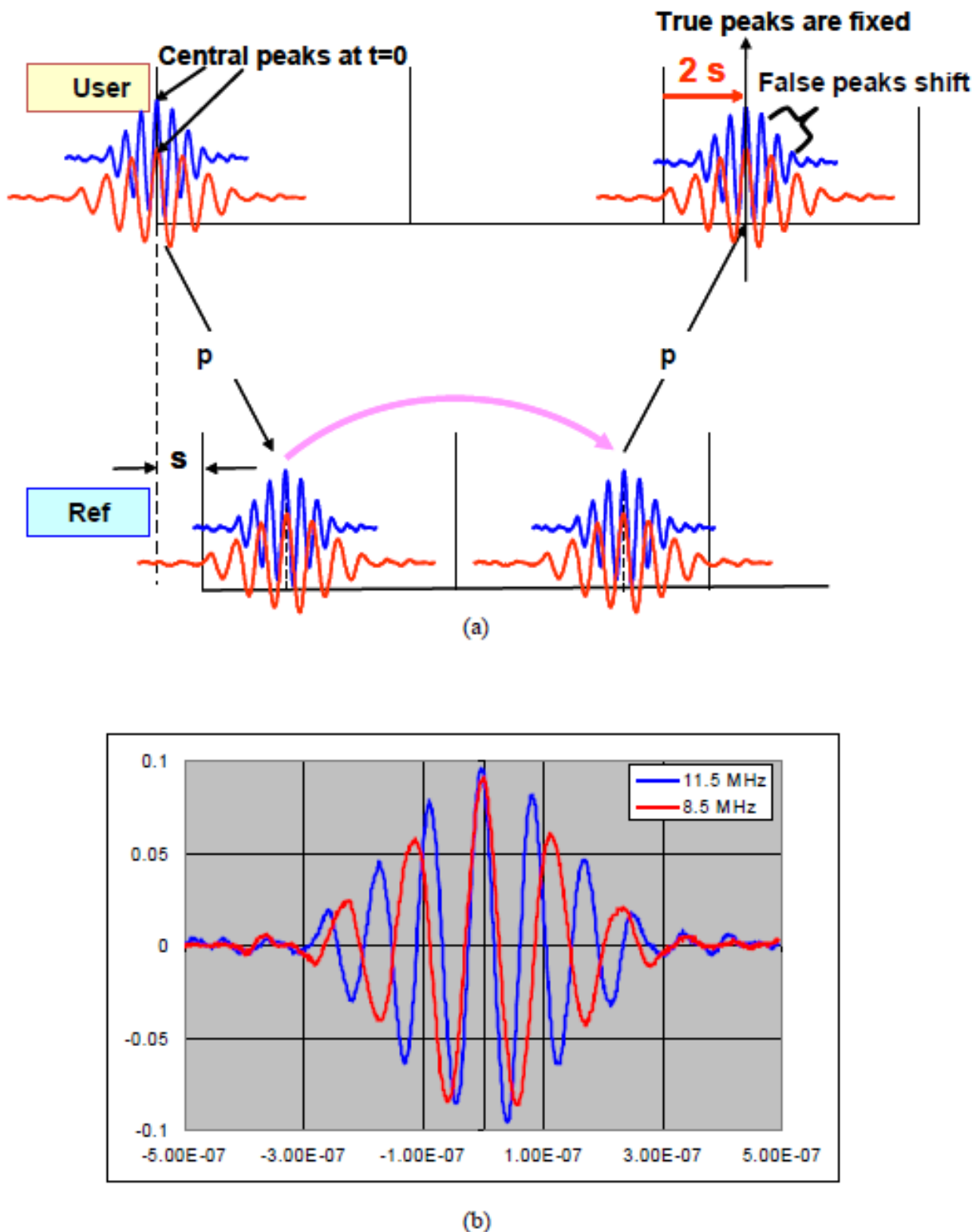


Figure 3. Mitigation of integer ambiguity by frequency dithering.

## IV. MULTIPLE USER SUPPORT

Unlike the conventional two-way systems, T<sup>3</sup>R system does not require coordination between nodes and data exchange. Moreover, owing to its multipath-tolerant property, directional antennas are not necessary. The reference node simply repeats the three step process, detection, time reversal, and retransmission in a pre-agreed period T, without having to pay attention to individual users. This provides each user node with a freedom, within limits, to choose its own waveform, carrier frequency, and delay. Therefore, conventional multiplexing schemes (time-, frequency-, and space-division if the reference node consists of an array of elements) may be used to support multiple users simultaneously.

To investigate the capability of the T<sup>3</sup>R system to support multiple users even in a multipath environment, we set up 3 nodes - one reference node and two user nodes. As shown in Figure 4(a), top left, the user nodes are separated from the reference node by about 800 ft, and along the direct beam path, there are several other buildings. Moreover, omni-directional vertical antennas are used for all the nodes. Therefore, one may expect multipath interference.

In this test, a frequency-division multiplexing scheme was used to support multiple users. Each user has a unique carrier frequency and a bandpass filter (BPF) installed within the node (top right corner of the figure).

In this experiment the sequence of events proceeded as follows. User 1 sends its signal with a carrier frequency  $f_1$ , and the returning signal from the reference node is passed through BPF1 and is used to estimate time offset,  $s(1, \text{meas})$ , with respect to the reference node. Likewise, user 2 estimates  $s(2, \text{meas})$  using its own carrier frequency,  $f_2$ . The difference between the two measured values is the measured time offset between the two user nodes and is denoted as  $s(1-2, \text{meas})$ .

To obtain the true time offset between the two user nodes,  $s(1-2, \text{true})$ , the trigger signals from both user nodes were directly connected and compared on a separate oscilloscope. Although the two user antennas are separated by about 100 ft, the instruments including the AWGs were in the same control room, allowing direct access to the trigger signals.

Figure 4(b) shows the experimental results. The blue curve shows the measured time offset,  $s(1-2, \text{meas})$ , and the green curve shows the true time offset,  $s(1-2, \text{true})$ . The difference between the measured and true values is the measurement error of our T<sup>3</sup>R system and is plotted in red color. The rms error of 0.31 second was obtained over a 1000 second measurement period.

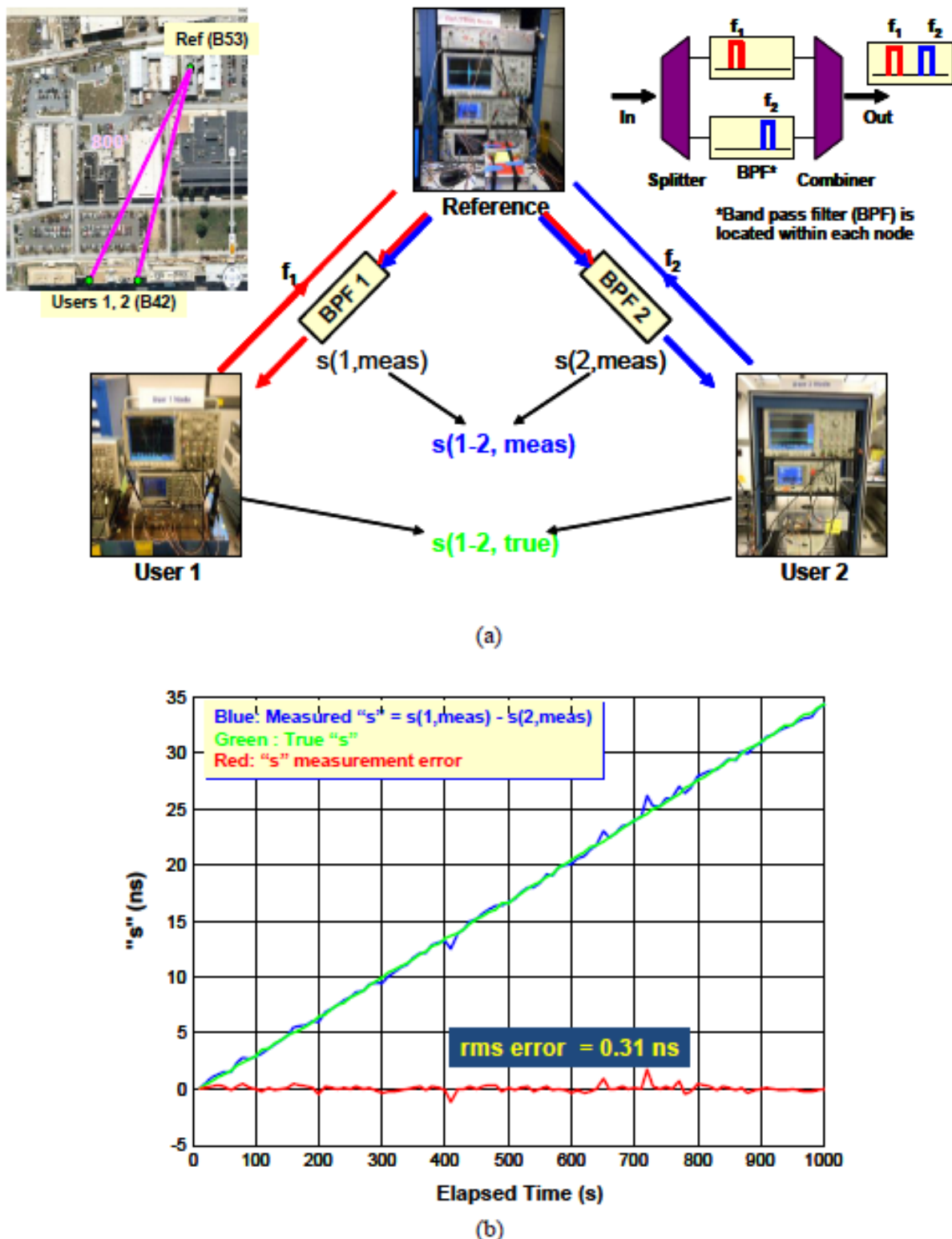


Figure 4. Multiple user support: (a) experimental setup; (b) results.

## V. TIME TRANSFER USING THE IONOSPHERE

Encouraged by the previous results, we challenged a more difficult problem – the ionosphere. We want to use the ionosphere as a mirror in the sky for long distance time transfer. However, the challenges include:

- 1) The ionosphere consists of multiple layers, hops, heights and polarization modes that are unknown and constantly changing.
- 2) The geomagnetic field causes the ionosphere to act as a non-reciprocal Faraday rotator, which causes both asymmetric propagation paths as well as fading.
- 3) Finally, unless the user uses a high transmit power (which may not be desirable for various reasons including low probability of intercept and portability), the signal can be much weaker than environmental noise, and thus time domain signal detection is difficult.

All the above effects may be ignorable for one way High Frequency time transfer with a modest accuracy (e.g. on the order of msec as with the conventional WWV) but are detrimental to obtaining a higher precision time transfer.

To investigate this technique we set up two nodes – one at the main site of NRL in Washington, DC, and another at the NRL Chesapeake Beach Detachment (CBD). These two sites are separated by about 30 miles with hills and forests, which block ground waves. To obtain a sky wave at this relatively short distance, Nearly Vertical Incident Skywave (NVIS) antennas, made of folded horizontal dipoles, were used. We confirmed that there are no noticeable ground wave effects between these two nodes.



Figure 5. Time transfer using the ionosphere.

## VI. ENVIRONMENTAL NOISE REDUCTION USING STROBOSCOPIC AVERAGING

In our case with a relatively low power transmitter with a maximum output of about 60W the environmental noise at the receiver is about 30 – 60 dB stronger than the real signal in time domain with a bandwidth of about 1 MHz. Various techniques were investigated to reduce the noise and increase SNR, such as narrow BPF, matched filtering, etc. In this study, we use the stroboscopic averaging method. This simple procedure is as follows:

- Signal is synchronously repeated at a pre-defined pulse repetition frequency (PRF).
- The noise is generally random and uncorrelated with the PRF.
- As a result, each frame will see the same signal and different noise.
- So, by a simple averaging process, noise becomes diminished, while signal is unaffected.

However, one should note that the PRF must be carefully selected to ensure that no integer multiples of the PRF fall into any major noise frequencies, determined from an analysis of local noise spectrum. The environmental noise is not necessarily white noise but has a number of man-made frequency components.

To test the effects, the linear FM signal with a tapering at both ends shown in Figure 6 was combined with the environmental noise through the same antenna and receiver. The noise was stronger than signal by about 30 dB. However, after the stroboscopic averaging, the noise had been removed, and the magnified view (right bottom) shows a clear signal with high fidelity. In this case, PRF was 1 kHz and 100 averages were used. So the processing time was 0.1 s. The built-in averaging capability of a conventional digital oscilloscope was used in this experiment.

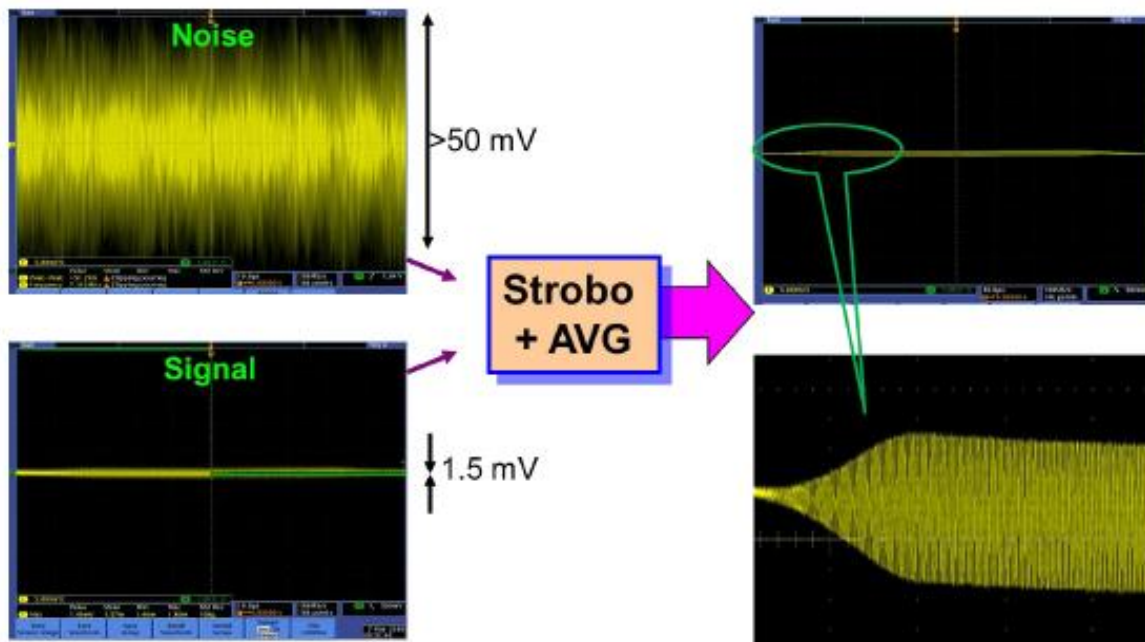


Figure 6. Environmental noise reduction by the stroboscopic averaging with the T<sup>3</sup>R.

## VII. “P”-INDEPENDENCE IN THE IONOSPHERE

As previously discussed, the ionosphere consists of several different layers, heights, and modes. However, for simplicity, let's consider the signal interaction with only two layers – the low E, and high F layers. When the signal is refracted from the same layer for both outgoing (user to reference) and returning (reference to user), as labeled as EE and FF in Figure 7(a), the path is reciprocal and the user will see the retuning signal at 2s, regardless of the structure of the ionosphere. However, some signal will be reflected from the E layer inbound, and F layer outbound, or vice versa, as labeled as EF or FE in the figure. In these cases, the correlation peaks will appear at an elapsed time other than 2s. For example, the peak EF will appear at  $2s + (p_F - p_E)$ , where  $p_F$  and  $p_E$  represent the propagation delays due to F and E layer, respectively. Obviously,  $p_F - p_E$  is  $p$ -dependent, and so as the ionosphere moves, the peak will shift in time. Therefore, these peaks through the non-reciprocal paths cannot be used to estimate the desired time offset, and so it is necessary to differentiate them from the desired reciprocal peaks. This is straightforward because the reciprocal peaks should be fixed at 2s, whereas non-reciprocal peaks will move, as explained.

When the ionosphere changes rapidly compared with the roundtrip time, invalidating the reciprocity, the reciprocal signals EE or FF will also shift. However, the amount of shift in this case is  $p_E(t) - p_E(t-\Delta t)$ , where  $\Delta t$  is a round trip time. Usually the amount of change in the height of the **same** particular layer during the round trip time is small, and thus the shift is small. However, for the non-reciprocal cases, FE or EF, the amount of shift is  $p_F(t) - p_E(t-\Delta t)$ , which can be large even for  $\Delta t = 0$  because it refers to the separation between two **different** layers.

Figure 7(b) shows an experimental result obtained from the two test sites described previously. It consists of 12 frames, and each frame was taken every 10 minutes over two hours. Each frame shows the signal strength as a function of time from 0 (center) to 1 ms (far right), and is folded to left starting from 1 ms (far left) to 2 ms (center), and so on.

One can clearly see that the true correlation peaks through reciprocal paths remain fixed at 2s over the entire two hours. Whereas, the side peaks through non-reciprocal paths move. Therefore, one can easily identify the desired peak through reciprocal paths.

One beauty of our “ $p$ ”-independence is that a user can measure the time offset against the remote reference node directly from the figure by simply measuring the true peak location and dividing by 2, without having to have any pre-knowledge on the structure of the ionosphere or to contact the remote nodes. However, although the peak remains fixed in time, the amplitude of the peak varies as a function of time due to fading effects.

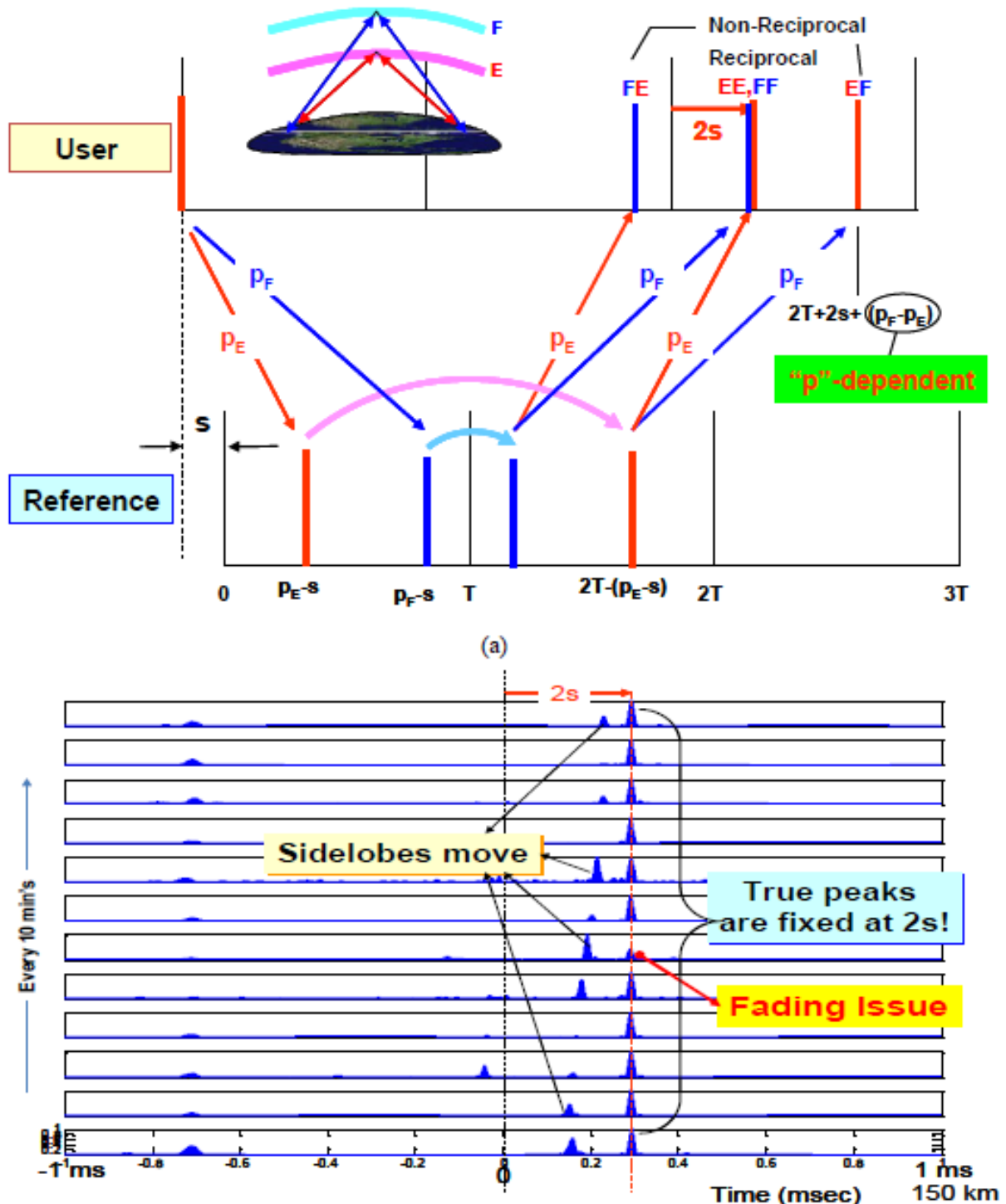


Figure 7. “p”-independence in the ionosphere.

## VIII. MITIGATION OF THE IONOSPHERIC NON-RECIPROCITY

The fading effects shown in the previous section is related with the ionospheric non-reciprocity, which has two components - temporal and spatial- as illustrated in Figure 8(a).

Temporal non-reciprocity effects are simply due to the change in the structure and irregularities of the ionosphere and so can be reduced by simply reducing the round-trip time. In our previous experiments schematically shown in Figure 2(a), the round-trip time was around 5 seconds, which was required to digitize the signal by an oscilloscope, read in the values to a PC, time reverse by the PC, and reload the time-reversed waveform into an AWG. Besides, we used slow electro-mechanical switches with a switching time of around 15 ms. We are currently reducing the round-trip time to around 10 ms by using FPGA-based time reversal processor and fast solid state switches with a switching time of 40  $\mu$ s.

Even though there are no temporal changes in the ionosphere during the round trip time, the geomagnetic field surrounding the earth causes the signal polarization to rotate due to the Faraday effect, which is a well-known spatial non-reciprocal effect. To cope with the Faraday effect, we transmit the signal along one of the characteristic modes of the ionosphere, e.g. right circular (RC) polarized beam using a polarization diversity antenna and a 90° phase shifting coupler. The polarization diversity antenna consists of two orthogonally oriented NVIS antennas. Since the RC polarization is an eigen mode, the state of polarization does not change as the signal propagates through the ionosphere, and the signal will follow along the “O” mode path. However, when the signal is reflected from the TRM, RC polarization will become LC due to the mirror inversion. As a result, the reflected beam will follow the “X” mode path, which is the worst non-reciprocal case. To avoid this problem, the sense of the circular polarization of the antenna at reference node must be quickly switched from LC to RC before retransmission. Similarly, the user also needs to change the sense of circular polarization before receiving the signal.

Figure 8(b) shows a schematic diagram of the entire T<sup>3</sup>R system currently under construction. Compared with the previous system shown in Figure 2 (a), an oscilloscope and an AWG in the reference node are replaced with FPGA electronics. Also, a single linear antenna at each node is replaced with a polarization diversity antenna with 90° coupler and sense switches, as explained before. All the switches are replaced with fast solid state switches.

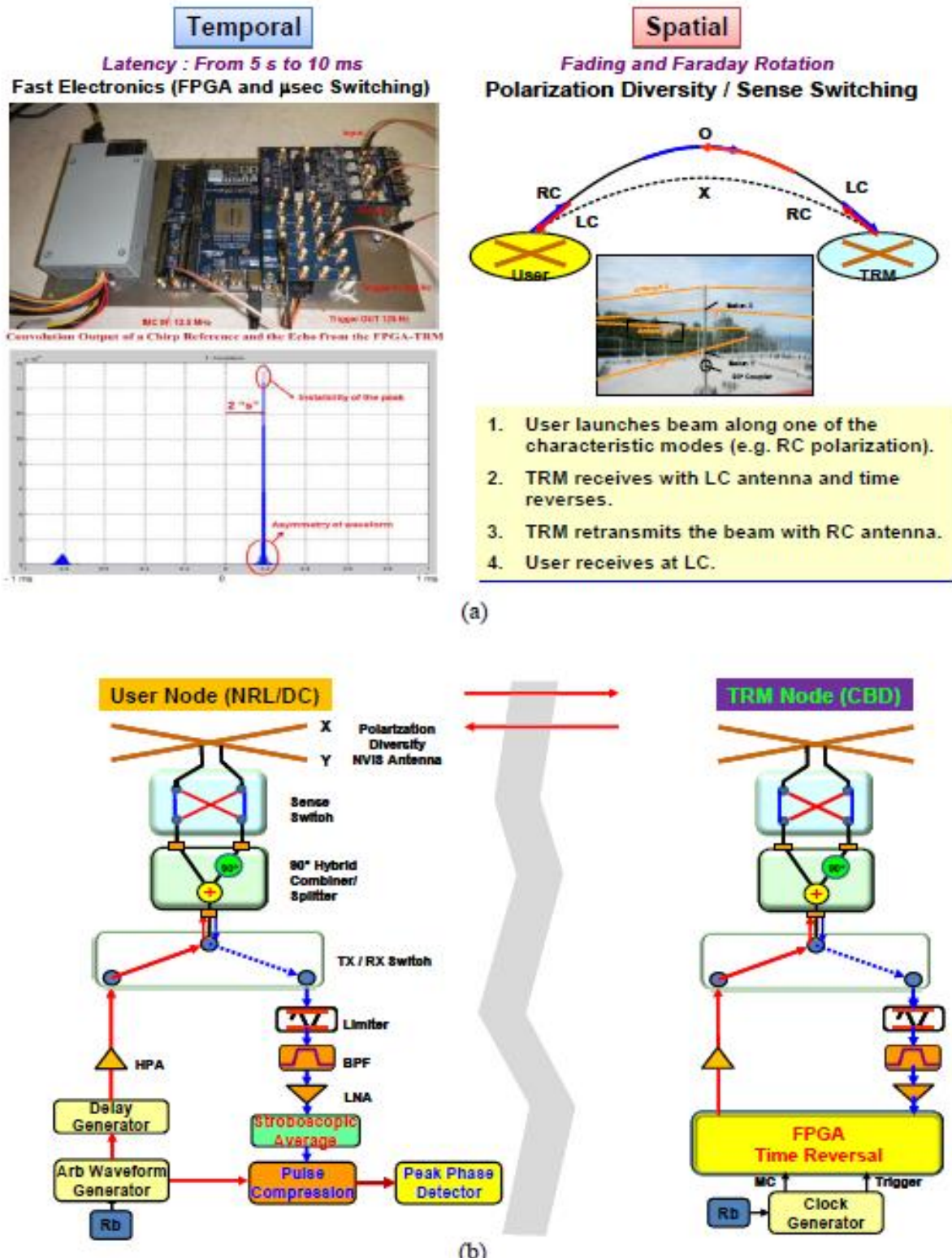


Figure 8. T<sup>3</sup>R to mitigate the ionospheric non-reciprocity effects: (a) our solution; (b) schematic diagram.

## CONCLUSION

We have introduced a new time transfer method T<sup>3</sup>R. By operating time reversal at a pre-agreed period, one can effectively decouple propagation delay and time offset, and extract only the desired time offset, leading to “*p*”-independence.

To validate the concepts, we experimentally demonstrated several key features including “*p*”-independence, mitigating integer ambiguity with frequency dither, multiple user support even in a multipath environment, long-distance time transfer using the ionosphere.

We are currently investigating a way to cope with the ionospheric non-reciprocity, as shown in Section VIII. We are also considering the extension of the T<sup>3</sup>R concept to various transmitting media (FSO, fibers, etc.) and waves (other electromagnetic waves or acoustic waves). In the future we hope to explore the possibility of T<sup>3</sup>R on a mobile platform.

Certain commercial equipment, instruments and materials used in this paper do not represent any recommendation or endorsement by Naval Research Laboratory.

## ACKNOWLEDGMENT

This work is currently supported by DARPA-STO. Earlier portions of this work were funded as part of the NRL Base Research Program.

The authors would like to thank Dr. Joseph D. White for the many valuable suggestions and Mr. David B. Young for a timely implementation of an FPGA-based TRM.

## REFERENCES

- [1] J. Levine, 2008, “A review of time and frequency transfer methods,” **Metrologia**, **45**, S162-S174.
- [2] M. Fink, 1999, “Time-Reversed Acoustics,” **Scientific American**, pp. 91-97.
- [3] A. Yariv, 1978, “Phase Conjugate Optics and Real-Time Holography,” **IEEE J. of Quant. Electronics**, **QE-14**, 9, 650-660.
- [4] C. C. Cutler, R. Kompftner, and L.C. Tillotson, 1963, “A Self-Steering Array Repeater,” **Bell System Technical Journal**, September, 2013-2032.
- [5] H. Lu, H. Wang, A. Aissa-El-Bey, and R. Pyndiah, 2010, “Underwater Time Service and Synchronization Based on Time Reversal Technique,” Shallow Water Acoustics, AIP Conference Proceedings Series, #1272, December 2010, Springer-Verlag, New York, LLC.
- [6] E. G. Paek and J. Choe, 2009, “TIME TRANSFER METHOD AND SYSTEM,” patent pending, US Docket No: 10226-US1.

- [7] E. G. Paek and J. Choe, 2009, “*Over-the-horizon radars with multipath-enabled super-resolution using time-reversal,*” in Proceedings of the 2009 IEEE Radar Conference, 4-8 May 2009, Pasadena, California, pp. 1-6.